Maple algorithm for damping quality of anechoic chambers evaluation

Martin Pospisilik, Rui Miguel Soares Silva, and Milan Adamek

***Abstract*—** Anechoic and semi anechoic chambers are among the necessary equipment that is needed for testing of devices for their electromagnetic compatibility or for experiments with electromagnetic field emitters, receivers, shielding and many more devices. As they require shielding for their proper operation, undesirable reflections occurring inside them are a natural consequence that must be eliminated by suitable absorbers. Naturally, the reflections cannot be eliminated absolutely in any case, but the aim of the constructers of such chambers is always to minimize them as well as possible. As the constructions of the chambers differ, each of them shows different resonant frequencies and standing waves displacement, although it complies with the standards for electromagnetic compatibility measurement. This phenomenon increases in its importance when the chamber is intended to be used for scientific purposes. In some cases, the knowledge of its behavior is crucial for various experiments. Because the standing waves caused by the reflections inside the chamber manifest themselves as resonant peaks occurring in the frequency response measurement, one of the possibility of evaluation of the quality of the reflections' damping is to identify the resonant peaks and calculate the Q-factor of the chamber, considering it acts as a cavity resonator. As cavity resonators usually show very high Q-factors, the lower value is obtained, the better damping by the absorbers in the chamber is ensured. One of such approaches to evaluate the real chamber that is being operated at Tomas Bata University in Zlin, using an algorithm implemented in Maple software, is described within the framework of this paper.

***Keywords*—**Anechoic chamber, electromagnetic compatibility, cavity resonator, reflections damping

I. Introduction

With the increasing demand for testing various electrical devices for their electromagnetic compatibility, the importance of semi anechoic chambers is currently increasing. The semi anechoic chambers are constructed in that way so they simulated measurements in open space area, with no reflections from lateral directions and from above, but with defined reflections from the ground. Therefore the semi anechoic chambers are equipped with absorbers displaced around their walls and ceilings while their floor is made of conductive material (metal) and being uncovered by any material that would affect the natural reflections. These chambers are suitable for both main groups of electromagnetic compatibility radiation measurements – the electromagnetic susceptibility (EMS), consisting of exposure of the tested devices to the electromagnetic field radiated by the antenna, and also the electromagnetic interference (EMI), consisting of measurement of the electromagnetic field that is being emitted by the tested device. [3]

When the antenna measurements are operated on for other scientific reasons, the floor of the semi anechoic chamber can also be covered by the absorbers. In this case the absorbers are installed at are reflecting surfaces inside the chamber and the chamber is called fully anechoic. [3]

However, in both cases, there is a demand for effective shielding of the room inside the chamber from outer electromagnetic fields (GSM phones, radios, TV channels etc.) that would spoil the results of the measurement. Therefore the outer surfaces of the chambers are made of conductive materials (metal) and because of that they are highly reflective – not only for outer electromagnetic waves, but also for the inner ones. In this case the performance of the absorbers is crucial, although ideal absorbers with 100% effect at all frequencies cannot be constructed. When aiming to eliminate the occurrence of high amplitude standing waves at isolated places within the chamber, the shape of the chamber can also be irregular, pointing the respective reflections to various directions. This approach was also applied to the chamber that was analyzed within the research described in this paper. The description of the chamber is provided in the text below.

Because at Tomas Bata University in Zlin a semi anechoic chamber is used, its behavior was studied by mapping the electric field distribution within its space, especially at the frequencies that are expected to be close to the dominant modes of the chamber. The results of rough mapping of the spectrum inside the chamber are described in the framework of this paper as well as the algorithm that was used to detect the resonant peaks in the frequency response of the chamber at different points. The goal of this research is to find a simple method of evaluation of the behavior of the absorbers inside the chamber on the basis of the Q-factors calculated for the resonance peaks that occurred at different places of the chamber. With the

This work was supported in part by the European Regional Development Fund under the project CEBIA-Tech No. CZ.1.05/2.1.00/03.0089 and by OPVK project CZ.1.07/2.3.00/30.0035.

Martin Pospisilik is with Faculty of applied informatics, Tomas Bata University in Zlin, Nad Stranemi 4511, 76005 Zlin, Czech Republic (corresponding author, phone: +420 606 417 702; e-mail: pospisilik@fai.utb.cz)

Rui Miguel Soares Silva is with Polytechnic Institute of Beja, Campus do Instituto Politécnico de Beja Rua Pedro Soares, 7800-295 Beja, Portugal (e-mail: ruisilva@acm.org)

Milan Adamek is with Faculty of applied informatics, Tomas Bata University in Zlin, Nad Stranemi 4511, 76005 Zlin, Czech Republic (corresponding author, phone: +420 606 417 702; e-mail: adamek@fai.utb.cz)

algorithm described in this paper, once any changes in the configuration of the chamber are applied, the measurement can be processed once again and from the measured results the changes of the chamber's behavior can quickly be visualized.

II. Problem Formulation

The goal of the research was to propose an algorithm that would analyze the big amount of frequency responses measured inside the anechoic or semi anechoic chamber at different places and provided information on the quality of damping of the inner reflections. Evaluation based on calculated Q-factor was chosen. In the text below, the problem of reflections as well as the reasons for choosing this method is described.

A. Default space configuration for EMC measurements

As stated in the text above, the simplest configuration for Electromagnetic interference measurements according to the CISPR 16-1 standard is an Open Area Test Site the configuration of which is depicted in Fig. 1.

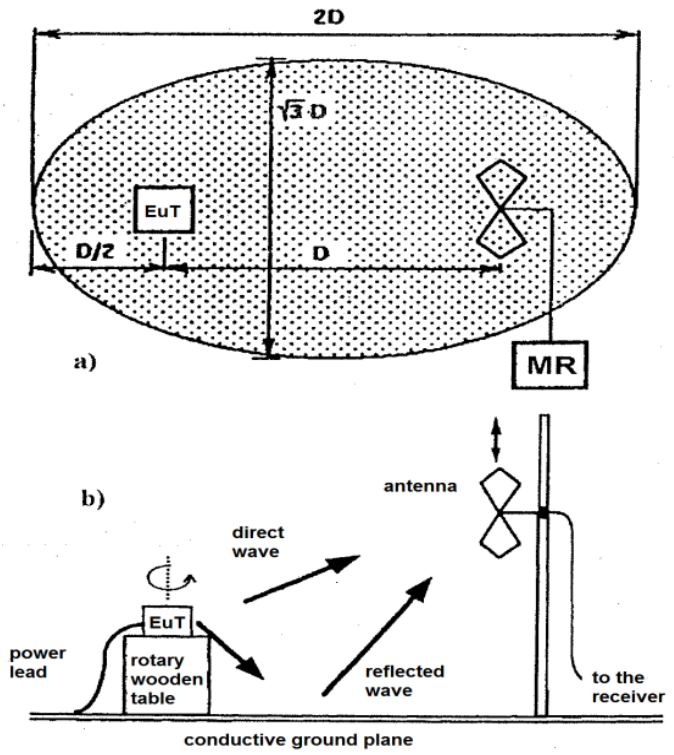

Fig. 1 Generic open area test site configuration [3]

With the accordance to the standards, the distance measurement D is usually 3, 10, 30 or 100 m. The accuracy of the measurement increases proportionally to the distance, but with the increase of the distance, the level of disruptive ambient fields would become critical. Sufficient attenuation of the reflected waves is reached when highly reflective surfaces are kept behind the area of the ellipse depicted in Fig. 1. To ensure the reproducibility of measurements, additional specifications of the shape of the grounded metal flooring at the site are prescribed by relevant standards [3]. Then the height of the measurement antenna is adjusted in several steps and the Equipment under Test (EuT) is rotated as well in order to find the worst case of interference.

B. Application of semi anechoic chambers

In order to achieve relevant results, the level of ambient disruptive fields should be at least 20 dB lower than the level of the field radiated by the EuT [3]. Currently, this condition is not easy to be achieved as there are many sources of electromagnetic fields almost at all places inhabitated by people. Therefore, electromagnetically shielded chambers are used to process the measurement in practice. Unfortunately, the shielded chamber acts as a cavity resonator. Its resonant frequencies can be calculated according to the following equation:

$$f_{ijk} = \frac{c}{2\pi\sqrt{\mu_r \varepsilon_r}} \sqrt{\left(\frac{i\pi}{L}\right)^2 + \left(\frac{j\pi}{H}\right)^2 + \left(\frac{k\pi}{W}\right)^2} \quad (1)$$

Where:
c – field propagation velocity [m/s],
μr – relative permeability [-],
εr – relative permittivity [-],
i, j, k – wave indexes (case i = j = k = 0 is forbidden),
L – box length [m],
H – box height [m],
W – box width [m].

As a result of this, a great variety of resonant frequencies inside the chamber occurs. A typical frequency response of an undamped chamber is depicted in Fig. 2.

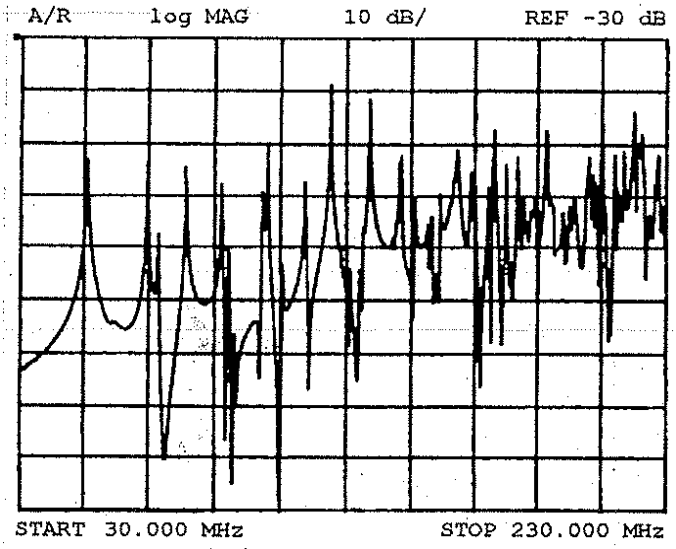

Fig. 2 Typical frequency response of undamped semi anechoic chamber [3]

The number of modes occurring within the chamber can be high, but usually the most significant are those of low i, j, k numbers. Several visualizations of energy displacement for various modes are provided in the figures below. It was obtained by simulation applet [11]. The detailed description on the modes can also be found in [1].

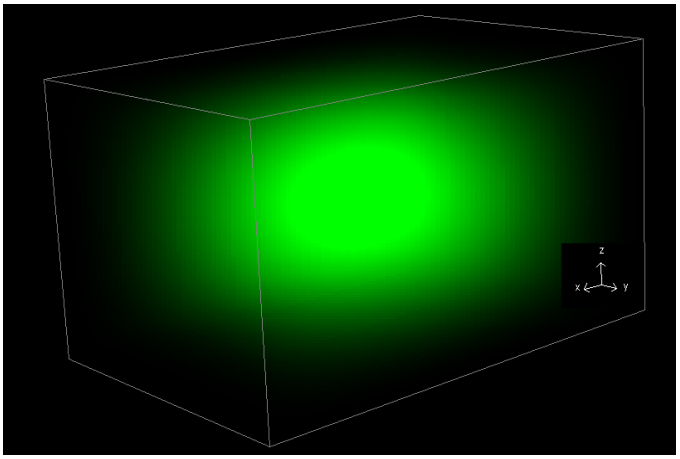

Fig. 3 Energy displacement visualisation for mode TE_{101}

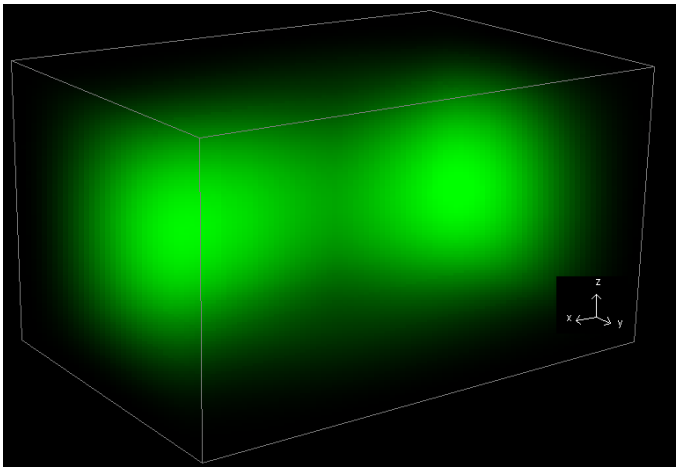

Fig. 4 Energy displacement visualization for mode TE_{121}

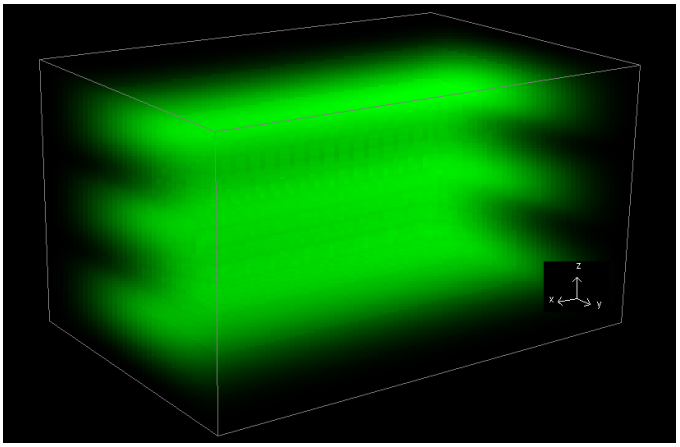

Fig. 5 Energy displacement visualization for mode TE_{013}

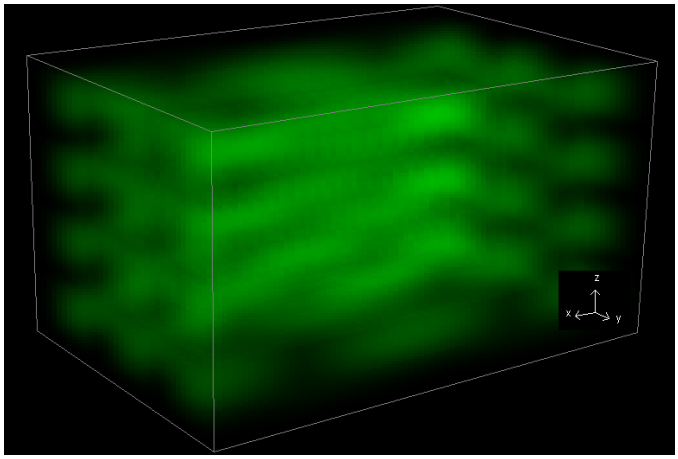

Fig. 6 Energy displacement visualization for mode TE_{234}

As stated above, the damping is ensured by absorbers that are displaced around the reflective surfaces inside the chamber. In most cases a combination of two types of absorbers is used:

- Flat ferrite absorbers that can be tuned to desired frequency and damping factor by their thickness and perforation,
- Pyramidal absorbers the performance of which is more wideband, but they are space demanding and in a compromise design not effective at lower frequencies.

The examples of their construction and performance are given below.

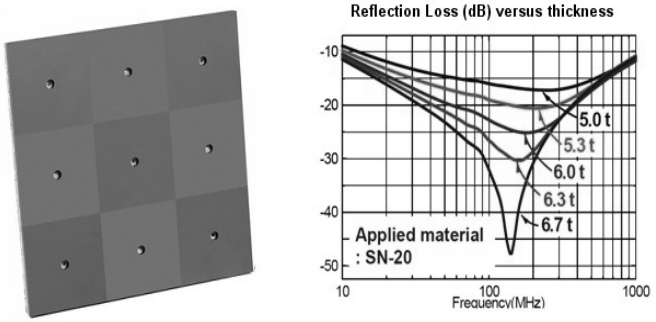

Fig. 7 Flat ferrite absorber and its performance (example) [2]

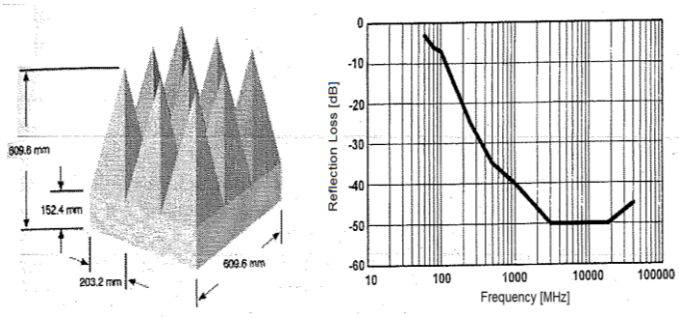

Fig. 8 Pyramidal absorbers and their performance (example) [3]

Based on the performance diagrams of the absorbers and the expectations, that the most striking standing waves are those of modes with low i, j, k numbers, there can be expected, that most problems with standing waves are likely to occur at lower frequencies. This was also confirmed by measurement and analysis that is provided in [10].

C. Experiment to be evaluated by the algorithm

The experiment to be evaluated by the algorithm is described in [10] in details as well as the obtained results. It consisted in measurement of frequency responses of the chamber in 15 different points. Semi anechoic chamber Frankonia SAC-3 Plus was employed in it, being declared by its manufacturer as a suitable unit for emission measurements according to EN 55022 / CISPR 22 class B and immunity tests according to IEC/EN 61000-3-4. The construction of the chamber is specific for its cylindrically shaped ceiling. The manufacturer claims that the dome shaped roof as well as its optimized absorber layout, with ferrite and partial hybrid absorber lining, minimizes the reflections in between 26 MHz and 18 GHz [4]. The frequency range of the experiment was from 10 to 80 MHz with the aim to drive the dominant mode of electrical field in this spectrum. Generic configuration of the chamber is depicted in Fig. 9.

According to the documentation, the internal dimensions of the chamber are listed in Table 1.

Table 1. Dimensions of the chamber

Length	9,680 mm
Width	6,530 mm
Height	9,500 mm (maximum)
	6,000 mm (minimum)

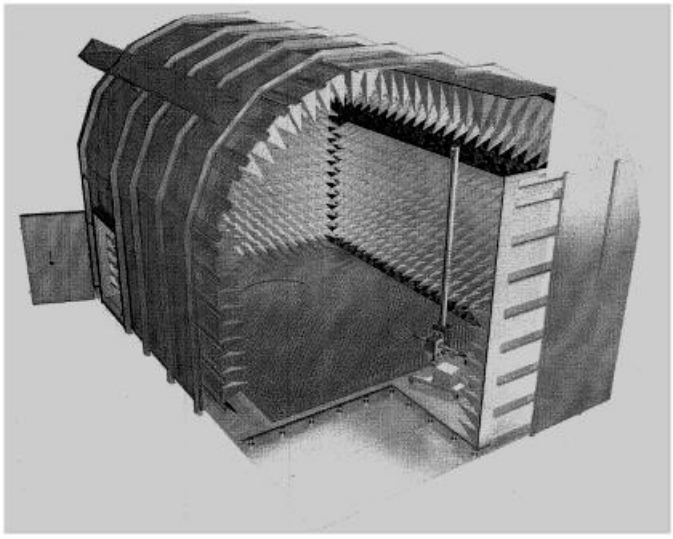

Fig. 9 Semi anechoic chamber Frankonia SAC 3 – plus [4]

The height of the chamber varies according to position, as the ceiling is of cylindrical shape. The maximum height is in the longitudinal plane of the centre of the chamber, the minimum height is near the longer walls of the chamber. As the chamber is equipped with cone absorbers, the internal area is effectively restricted to approximately 8,120 x 5,150 mm.

The configuration of the points of measurement is depicted in Fig. 10. Transmitting antenna (ANT) was an omnidirectional monopole fed with the power of 0 dBm. At the positions (A) to (O) the mutual distances of which was 1,300 mm, Rohde & Schwarz omnidirectional spherical field probe HZ-11 was placed in order to measure the frequency response of the chamber to the transmitted electrical field. The field probe was always placed at a height of 1,500 mm.

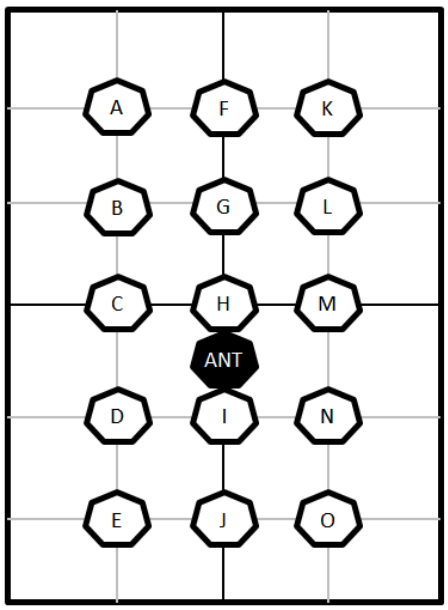

Fig. 10 Displacement of the measurement points in the chamber

As a result, 15 frequency responses in the range from 10 to 80 MHz were obtained. The dominant mode as well as several higher modes was observed in them, in compliance with the expectations gained from calculations that were based on the dimensions of the chamber. The chamber acted mainly as a cuboidal resonator. The comparison of the measured and calculated dominant frequencies is provided in the Table 2. The set of measured frequency responses is depicted in Fig. 11. The diagrams are displaced according to the points of measurement as depicted in Fig. 10.

D. Demands on the algorithm

As obvious from the data obtained in the experiment (see [10] and/or Fig. 11 and Table 2), there is a numerous set of results to be analyzed. For each of the response, 625 points at the frequency axis are recorded, corresponding to the resolution of approximately 112.179 kHz. These data were obtained by the controlling software of the laboratory devices and exported into an Excel table. From this table they were extracted and visualized in Maple software in the form depicted in Fig. 11.

The main demand is to isolate the main peaks occurring in the diagrams of the responses and to evaluate these peaks by a simple set of values.

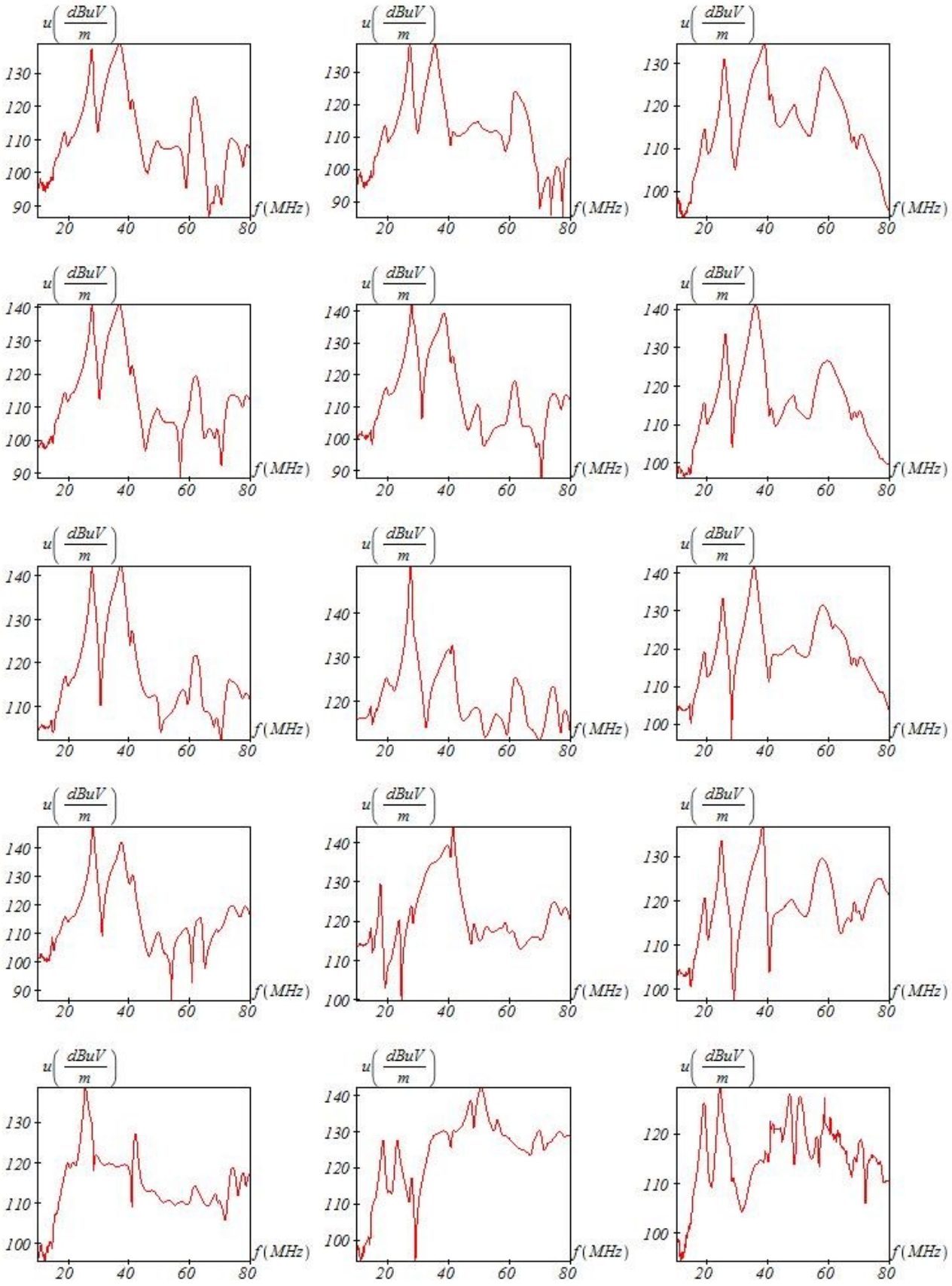

Fig. 11 Frequency responses sof the chamber measured at points (A) to (O) (see Fig. 9)

Table 2 Comparison of dominant frequencies identified by the measurement and expected on the basis of calculations

Point of measurement	Frequency [MHz]	Closest mode	Deviation from the calculated frequency [MHz]
A	36.81	TE111	- 0.34
B	36.81	TE111	- 0.34
C	37.15	TE111	+ 0.02
D	28.17	TE101	+ 0.47
E	25.71	TE101	- 1.99
F	35.58	TE111	- 1.55
G	27.95	TE101	+ 0.25
H	27.61	TE101	- 0.09
I	41.41	TE102	+ 2.70
J	50.83	TE201	+ 2.63
K	38.72	TE102	+ 0.01
L	36.03	TE111	- 1.10
M	35.46	TE111	- 1.67
N	38.27	TE102	- 0.44
O	24.25	TE101	- 3.45

Such a demand can easily be met by isolating the peaks and treating them as resonant frequencies of an oscillating circuit. Then, each of the peaks can be described by two values, the frequency and Q-factor.

Generally, one of the approaches describes the Q-factor as follows: By applying 3 dB criteria, the quality factor of the resonant element can be calculated as [7]:

$$Q = \frac{f_0}{B_{3dB}} \tag{2}$$

In (8) f_0 means the resonant frequency and B_{3dB} means the bandwidth in which the power decrease in neighbourhood of the resonant frequency is equal to 3 dB. Once the frequency response curve is known, this approach can be applied for the purposes of the evaluation described in this paper.

Secondly, by application of the approach described above, considerable data reduction can be achieved, which simplifies the evaluation of the quality of the chamber's damping.

III. Description of the Algorithm

As stated above, the algorithm should identify and isolate peaks in the frequency response and calculate Q-factor for them. Once a reduced set of data is obtained, it can also be visualized. By plotting the data into one diagram, also the position of the peaks on the frequency axis of the responses measured at various points can be compared.

A. Implementation

First of all, the data from the Excel table are loaded in a form of an array. The dimension of the array is 15 x 625, as there are 625 measured points at 15 different palaces. Because the frequency range is known (10 to 80 MHz), the frequency for each point can be calculated as follows:

$$f_i = f_{min} + \left((i-1) \frac{f_{max} - f_{min}}{N-1} \right) \tag{3}$$

Where:
f_i - frequency corresponding to the i-th measured point [Hz],
f_{min} – frequency at which the measurement started [Hz],
f_{max} – frequency at which the measurement finished [Hz],
i – position of the point of the measurement,
N – total number of the points of the measurement.

For the purposes of the research described in [10], the parameters are as follows: $f_{min} = 1 \cdot 10^6$ Hz, $f_{max} = 8 \cdot 10^6$ Hz, N = 625. The calculated relevant frequencies are loaded into a separated vector.

Then the whole rest of the algorithm is included in a cycle running from 1 to 15, because each frequency response is processed separately.

In each of the run of the cycle, the following steps are processed. Firstly, all peaks are identified. Every value that is higher than its predecessor as well as its successor is recognized as a peak. To store these peaks, a new vector P (1..625) is created and the value of the peak is stored in it at the position corresponding to its frequency. For the frequencies at which no peak was detected, the value P[i] is set to 0. The total number of detected peaks is then stored in a variable NumPks.

Secondly, from the set of the local maxima only the relevant (substantial) peaks must be isolated. Only those peaks are marked as relevant, that comply with the following criteria:

- On both sides (left, right) of the peak a point can be find, the level of which is at least 3 dB lower (3dB criteria). The positions of such points are stored to variables LeftLimit and Right Limit.
- Concurrently, no point between LeftLimit and RightLimit is of a higher level than the examined peak.

Once the position of the peak is known as well as the position of the closest points to the peak that comply to the 3dB criteria, the Q-factor for this peak can be calculated, using a modification of formula (2):

$$Q_i = \frac{i_{Pk}}{i_{RightLimit} - i_{LeftLimit}} \tag{4}$$

Where:
Q_i – Q-factor calculated for the i-th frequency point,
i_{pk} – position of the identified peak,
$i_{RightLimit}$ – positon of the first point to the right from i_{pk} that comply with the 3dB criteria.
$I_{LeftLimit}$ – positon of the first point to the left from i_{pk} that comply with the 3dB criteria.

As a result of the computation, a new array of Q-factors is obtained, containing zeros at the positions, where no relevant peaks were detected, and values of calculated Q_i at the positions where the peak detection was successful. Finally, this array can

be visualised according to the current needs.

The algorithm flowchart is depicted in Fig. 12.

B. Application

The algorithm was applied to the data obtained by experiment described in [10]. First of all, the detection of all possible peaks was tested. An example of obtained plot for arrays V and P is depicted in Fig. 13.

Subsequently, filtering of substantial peaks was implemented. The example of the result gained from the same data is depicted in Fig. 14.

Finally, a graph of Q-factors in one iteration was obtained. This graph is depicted in Fig. 15.

The result of processing all data (NoOfResponses = 15) is depicted in Fig. 16.

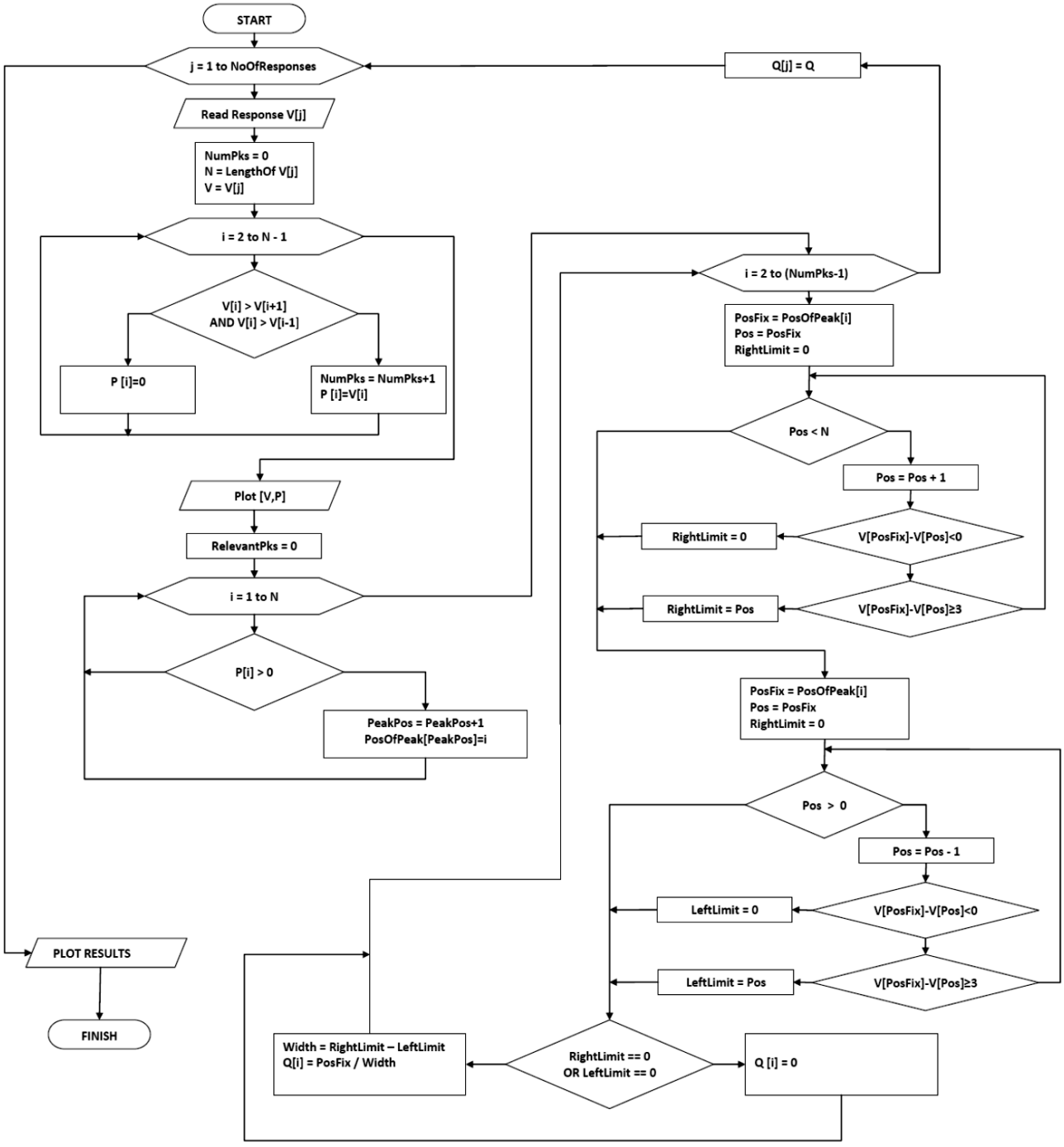

Fig. 12 Maple algorithm flowchart

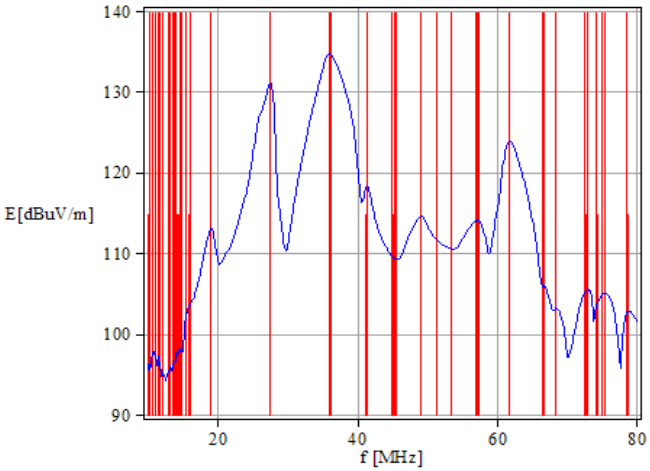

Fig. 13 Example of all potential maxima detection in one frequency response array

The set graph at Fig. 16 shows maxima detections and Q factor calculations for all 15 frequency responses obtained within the experiment [10]. From their position in the [x,y] space it can be observed how the resonant frequencies differ in space and how good is their damping.

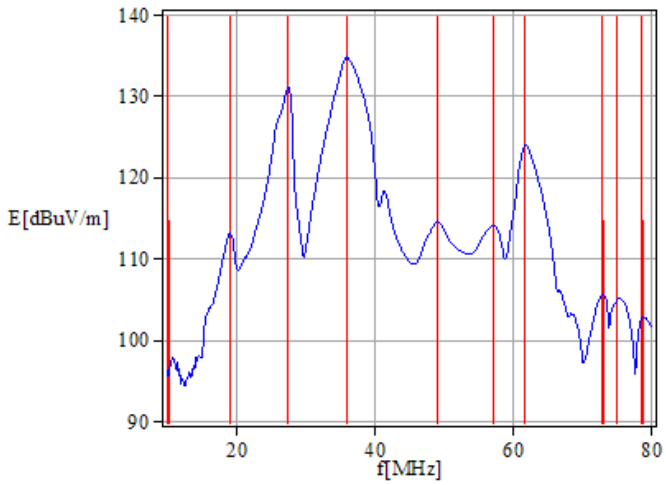

Fig. 14 Filtered maxima detection (only substantial peaks)

IV. Conclusion

Within this paper a description of one of possible methods of evaluation of the quality of internal damping of semi anechoic and anechoic chambers is provided. This method is based on automated search for resonant peaks obtained from frequency responses measured at different positions within the space of the chamber and calculation of equivalent Q factor for a resonant circuit that would show the same response.

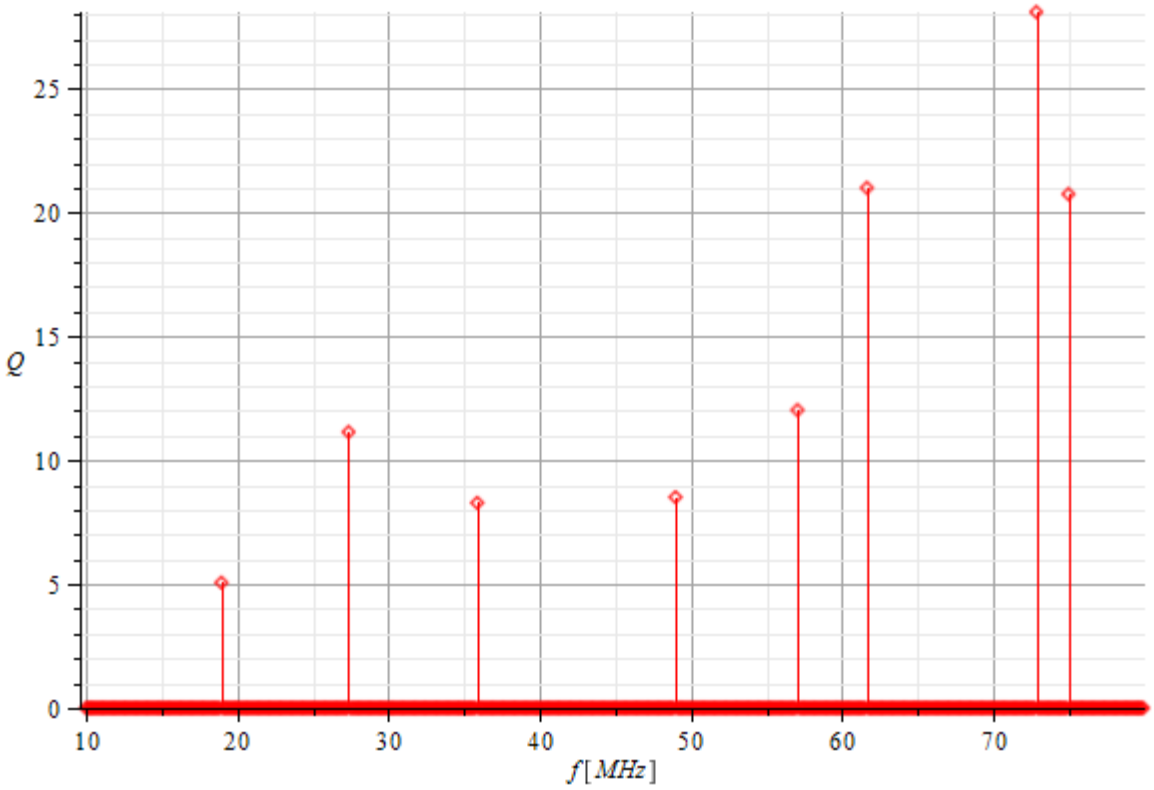

Fig. 15 Results of Q detection for resonant peaks obtained from one frequency response

Theoretically, if no power losses occur, the Q-factor of a cavity resonator would reach unlimited values. In practice, for example according to [12], the Q-factor of resonating cavity is limited by three different power loss mechanisms:

- Power losses in the walls of the cavity caused by their finite conductivity,
- Power losses caused by any dielectric material that fills the cavity,
- Power losses caused by wall surfaces' inhomogenities (holes, rough surface etc.) and other external impacts.

According to [12] the total Q-factor can be expressed as follows, taking into account all above listed mechanisms:

$$Q_{total} = \frac{1}{\frac{1}{Q_c} + \frac{1}{Q_D} + \frac{1}{Q_{ext}}} \quad (5)$$

Where Q_C is a cavity Q-factor determined by the conductivity of its surfaces and geometry, Q_D is a Q-factor of the cavity determined by power losses in its dielectric filling and Q_{ext}

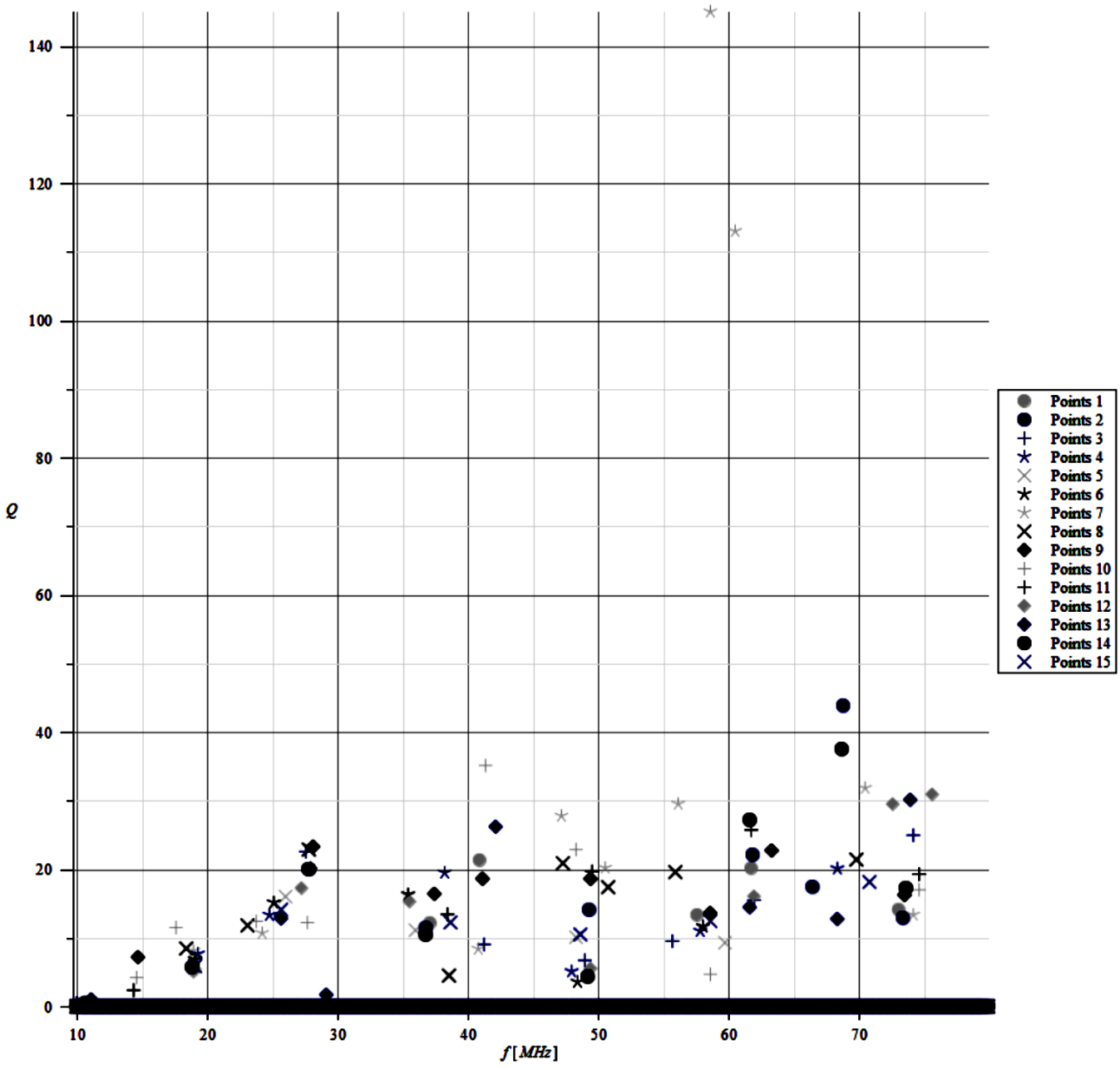

Fig. 16 Cumulative diagram for all resonances discovered in the chamber within the experiment [10]

comprises the impact of external factors (damping) to the Q-factor of the cavity. It is obvious, than the method presented in this paper cannot separate the three named mechanisms, but there is no need for it. The chamber is evaluated as a whole, according to its behaviour.

Whereas with the cavity resonators the higher Q-factor is, the better is the resonator, within the semi anechoic and anechoic chambers the situation is reversed. While precise cavity resonators reach Q-factors higher than 10,000 [13], with the semi anechoic or anechoic chamber, it is important to reach as low values as possible.

From Fig. 16 it is obvious that the Q-factor of most of the resonances is kept below 25. Isolated clusters of points can be observed in the proximity of calculated frequencies (see Table 2 or [10]). Only in two causes the high Q-factor values were detected (Q = 144.2 at 58.6 MHz and Q = 112.6 at 60.7 MHz). These values are ambiguous.

It is also interesting that the values of Q-factor tend to increase in accordance with the frequency. This effect was not expected, as the absorbers are generally supposed to perform better at higher frequencies.

For further research increased frequency range and number of measurement points is expected as well as different arrangement of the internal space of the chamber. However, from the results presented in this paper it can be seen that the construction of the chamber suppresses the resonances of the electrical field almost equally.

From the set of the obtained data, further information can be gathered, for example by means of evolutionary algorithms [14], [15]. For instance, for the required range of frequencies, a point at which the resonances are damped at most can be found.

REFERENCES

[1] S. Radu. (N/A). *Engineering Aspect of Electromagnetic Shielding,* Sun Microsystems. [online]. Available: http://ieee.rackoneup.net/rrvs/09/Engineering%20Aspects%20of%20Electromagnetic%20Shielding.pdf.

[2] Compliance Engineering. (2015). *Flat Ferrite RF Absorber: SFA version* [online]. Available: http://www.ferret.com.au/c/compliance-engineering/sfa-version-flat-ferrite-tile-rf-absorbers-from-compliance-engineering-n892923.

[3] J. Svačina, *Electromagnetic compatibility: Principles and notes [Elektromagnetická kompatibilita: Principy a poznámky],* 1st edition. Brno: Vysoké učení technické, 2001. ISBN 80-214-1873-7.

[4] Frankonia, (2012). *Anechoic Chambers / RF-Shielded Rooms*. [online]. Available: http://www.frankoniagroup.com/cms/fileadmin/shared/downloads/rooms%26chambers/Anechoic_Chambers.pdf.

[5] Rohde&Schwarz. (1999). *Probe Set HZ-11 for E and H near-field Measurements*. [online]. Available: http://cdn.rohde-schwarz.com/pws/dl_downloads/dl_common_library/dl_brochures_and_datasheets/pdf_1/Hz-11_en.pdf.

[6] Z. Trnka, *Theory of Electrical Engineering [Teoretická elektrotechnika]*, Bratislava: SNTL Alfa, 1972.

[7] Radio-Electronics (2015). *Quality Factor*. [online]. Available: http://www.radio-electronics.com/info/formulae/q-quality-factor/basics-tutorial.php.

[8] T.I Maris et al., "Electromagnetic field identification using artificial neural networks", In *Proceedings of the 8th WSEAS International Conference on Neural Networks*, Vancouver, British Columbia, Canada, June 19-21, 2007.

[9] M. Mann, B. Gutheil, J. Zastrau, P. Weiss, "Electromagnetic field measurements – Means of verification", In *Proc. of the 5th WSEAS/IASME Int. Conf. on Electric Power Systems, High Voltages, Electric Machines*, Tenerife, Spain, December 16-18, 2005.

[10] M. Pospisilik, J. Soldan, "Electromagnetic field distribution within a semi anechoic chamber", In *Proceedings of the 18th International conference on systems*, Santorini island, Greece, July 17-21, 2014, ISBN 978-1-61804-244-6.

[11] (N/A).(2014). [online]. Available: http://www.falstad.com/embox/.

[12] D. Pozar, *Microwave engineering*. 2nd edition. New York: John Wiley, 1998.

[13] COMSOL. (2014). *Computing Q-Factors and Resonant Frequencies of Cavity Resonators,* [online]. Available: http://www.comsol.com/model/download/156535/models.rf.cavity_resonators.pdf.

[14] J. Kolek, P. Varacha, I. Motyl*, Performance Evaluation of the SOMA Asychronously Parallel Distribution*, International Journal of Mathematics and Computers in Simulation, Volume 7, 2013, ISSN: 1998-0159.

[15] N. Bacanin, *Implementation and Performance of an Object-Oriented Software System for Cuckoo Search Algorithm*, International Journal of Mathematics and Computers in Simulation, Volume 6, 2012, ISSN: 1998-0159.